Journal of Materials Chemistry

Cite this: *J. Mater. Chem.*, 2012, **22**, 4066

www.rsc.org/materials

PAPER

Ionic liquid-nanoparticle hybrid electrolytes†

Yingying Lu, Surya S. Moganty, Jennifer L. Schaefer and Lynden A. Archer*

Received 20th October 2011, Accepted 4th January 2012
DOI: 10.1039/c2jm15345a

We investigate physical and electrochemical properties of a family of organic-inorganic hybrid electrolytes based on the ionic liquid 1-methyl-3-propylimidazolium bis(trifluoromethanesulfone) imide covalently tethered to silica nanoparticles (SiO_2-IL-TFSI). The ionic conductivity exhibits a pronounced maximum *versus* LiTFSI composition, and in mixtures containing 13.4 wt% LiTFSI, the room-temperature ionic conductivity is enhanced by over 3 orders of magnitude relative to either of the mixture components, without compromising lithium transference number. The SiO_2-IL-TFSI/LiTFSI hybrid electrolytes are thermally stable up to 400 °C and exhibit tunable mechanical properties and attractive (4.25V) electrochemical stability in the presence of metallic lithium. We explain these observations in terms of ionic coupling between counterion species in the mobile and immobile (particle-tethered) phases of the electrolytes.

Introduction

Among rechargeable/secondary battery technologies, lithium-ion batteries (LIBs) are considered the most promising for meeting emerging demands for high-capacity, cost-effective, reliable, and portable electrical energy storage.[1–6] Compared with nickel-metal hydride batteries (already successfully deployed in commercial hybrid electric vehicles (HEVs)), LIBs offer superior specific energy and power, which make them attractive for HEVs and plug-in hybrid electric vehicles (PHEVs). The most successful lithium-ion batteries employ a carbonaceous material such as graphite as the anode, which hosts lithium as LiC_6 in the charged state.[7] It has long been understood that removal of the carbon support to produce a so-called rechargeable lithium metal battery (LMB) would boost the energy storage capacity of the anode by more than a factor of 10 (from 360 mAh/g to 3860 mAh/g).[7,8]

Widespread adoption of such LMBs is impeded by safety concerns associated with uneven deposition of lithium on metallic substrates.[9,10] Over time, this uneven deposition results in growth of fibrillar or mossy lithium dendrites, which extend into the electrolyte and may eventually short circuit the cell. Because the most successful electrolytes in current use are aprotic liquids with high volatility and flammability, a short-circuited LMB can cause significant harm. An electrolyte capable of transporting lithium ions at comparable rates as in aprotic liquids, but which is non-flammable and non-volatile under normal cell operating conditions presents obvious safety advantages for a LMB.

Chazviel and co-workers have used theory and experiments to study the conditions required for lithium dendrites to initiate and propagate in a rechargeable LMB. The authors find that at high current density,[11,12] uneven lithium deposition is triggered by the space charge created as a result of a local deficit of anions near the cathode. The rate at which the dendrite front propagates is determined by the rate at which the space charge grows, which is set by the drift velocity of the anions migrating away from the cathode.[11] In this scenario, an electrolyte in which the anion is unable to move (single-ion conductor) or which is capable of selectively resupplying anions (supporting electrolyte) to the fluid near the cathode at a rate that matches or exceeds the rate at which anions are depleted, would prevent lithium dendrite growth and proliferation in a rechargeable LMB.

Ionic liquids are characterized by weak interactions between a large cation and a charge-delocalized anion. This feature produces unusual liquid-like transport properties, including ionic conductivity, at moderate temperatures. Ionic liquids have received consistent, intensive scientific interest due to their many attractive properties, such as low melting point, low vapor pressure, non-flammability, and good chemical and thermal stabilities. These properties make them suitable as solvents for various applications, including electrodeposition, catalysis, lubrication, energy, and bioscience,[13–16] and also make them very promising candidates as stable, non-flammable, non-volatile electrolytes for lithium battery applications.[17–19]

The ionic liquid 1-methyl-3-propylimidazolium bis(trifluoromethanesulfone) imide (C1C3imTFSI) has been studied extensively from applied and fundamental perspectives. The Henry's constant for carbon dioxide gas in C1C3imTFSI has

School of Chemical and Biomolecular Engineering, Cornell University, Ithaca, New York 14853, USA. E-mail: laa25@cornell.edu; Fax: +607-255-9166; Tel: +607-254-8825

† Electronic Supplementary Information (ESI) available: synthesis scheme, TGA data, power law frequency dependence of the moduli, tan(δ) VFT fit, lithium transference number data. See DOI: 10.1039/c2jm15345a

been reported to be 377 bar at room temperature, prompting investigations of the material as a substrate for carbon dioxide capture from low pressure gas streams.[20] C1C3imTFSI has also been investigated as a catalyst for the hydroformylation of alkenes,[21] as an attractive medium for electrodeposition of tantalum,[22] and as a solvent for extraction of aromatic compounds from aliphatic hydrocarbons.[23] Dlubek *et al.* studied C1C3imTFSI using PALS (position annihilation lifetime spectroscopy) and reported a glass transition at a temperature T_g = 187 K, a melting transition at a temperature T_c = 200 K, and a significant increase in the hole free volume fraction, which determines the temperature-dependence of viscosity, from 0.023 at 185 K to 0.17 at 430 K.[24] Xiao *et al.* have shown that the asymmetry of the C1C3imTFSI cation plays an important role in setting the low-frequency vibrational dynamics of the IL and in determining its relatively low melting point.[25] Pure C1C3imTFSI has been reported with an ionic conductivity of 7.42×10^{-3} S cm^{-1} at 30 °C.[26] When doped with the salt LiTFSI in a 1 : 1 molar ratio, the material is reported to exhibit a markedly lower ionic conductivity (*e.g.* 1.17×10^{-3} S cm^{-1} at 30 °C) due to the increased viscosity produced by the added salt. Notwithstanding ongoing efforts to optimize the materials conductivity and lithium transference number for battery applications, a Li/C1C3imTFSI-based P(VdF-HFP)/$LiFePO_4$ cell has been reported to exhibit stable performance even after 50 charge/discharge cycles.[26]

Despite these successes, ionic liquid electrolytes as a group suffer from two physical property limitations that make them unattractive for lithium battery applications. First, the fraction of the ionic conductivity of the electrolyte arising from mobile lithium ions (*i.e.* the so-called lithium transference numbers T_{Li^+}) are typically low, which makes cells assembled using IL electrolytes prone to polarization. For pyrrolidinium-based TFSI/LiTFSI and imidazolium-based TFSI/LiTFSI systems, lithium ion transference numbers below 0.2 are typical.[27–29] Frömling *et al.* reported that increasing the concentration of lithium salt in an IL electrolyte increases T_{Li^+} by weakening interactions between cations (Li ions) and the anions.[29] Second, most ILs exhibit low tensile and compressive strengths, which limits the form factors an IL-based lithium battery can take.

Significant recent efforts have shown that nanocomposites created by physically mixing bare and surface-functionalized nanoparticles with ILs open the way for hybrid ILs with mechanical properties comparable to typical solid polymer electrolytes.[30–36] And, several proof of concept studies have already been carried out to demonstrate their applications as "solid electrolytes" for solar cells,[30] electrochemical devices,[31] and color displays.[32,33] Ueno *et al.* reported that IL-based silica nanocomposite gels can be engineered to simultaneously exhibit high ionic conductivity and MPa-scale elastic moduli.[34] In a recent work, we reported a hybrid electrolyte composed of ZrO_2 nanoparticles functionalized with 1-butyl-3-undocylimidazolium bis(trifluoromethanesulfone) imide and doped to 1 M LiTFSI and showed that the material exhibits attractive electrochemical and mechanical features, including a high T_{Li^+}.[36] It was argued that jamming of the IL-tethered nanoparticles was responsible for the polymer-like mechanical properties and that the improved lithium transference numbers are a result of tethering of the positively charged ion in the IL.

Herein we report on hybrid electrolytes created by tethering the C1C3imTFSI to 7 nm SiO_2 nanoparticles. We show that the mechanical and electrochemical properties of the resultant SiO_2-IL-TFSI hybrid electrolytes can be facilely tuned by varying the amount of LiTFSI added. We also find that the ionic conductivity and T_{Li^+} can be simultaneously increased, relative to either of the pure solid salts by raising the content of SiO_2-IL-TFSI in the mixtures. In addition to these benefits, a jammed suspension of SiO_2-IL-TFSI provides a ready source of TFSI anions and as such can potentially play a critical role as a supporting electrolyte in a rechargeable LMB.

Experimental

Synthesis

Synthesis of SiO_2-IL-TFSI. Scheme 1 illustrates the procedure used to tether 1-methyl-3-propylimidazolium bis(trifluoromethanesulfone) imide to silica nanoparticles. 1-Methylimidazole (Aldrich) and (3-chloropropyl)trimethoxysilane (Aldrich) were dissolved in dimethylformamide (DMF) and stirred in an inert environment at 80 °C for 2 days. The reaction solution was purified *via* liquid extraction in ether and the solvent evaporated to produce the trimethoxysilane functionalized with the IL. The purity of product IL (1-methyl-3-trimethoxysilane imidazolium chloride) was verified by H-NMR Spectroscopy (Figure S1). To tether the IL to silica a simple water-based chemistry was used. In a typical reaction, LUDOX SM-30 colloidal silica (30 wt% aqueous suspension – 7 nm diameter) was diluted with DI water to create a 2 wt% aqueous suspension. To this suspension a solution containing 1.5 times excess (relative to what is needed to produce saturation coverage of the particles), 1-methyl-3-trimethoxysilane imidazolium chloride was added dropwise to the aqueous suspension and the mixture heated at 80 °C for 12 h with rapid stirring. Subsequently, the reaction temperature was increased to 100 °C to evaporate the water. The resultant SiO_2-IL-Cl was washed 3–4 times with ethanol and separated by centrifugation. A freeze dryer (lyophilizer) was used to remove the final traces of solvent from the SiO_2-IL-Cl nanoparticles.

The purity of the resultant SiO_2-IL-Cl particles was confirmed using proton NMR spectroscopy (Fig. 1(a)). Ion exchange in room-temperature water was used to substitute the chloride ion with the bis(trifluoromethanesulfone imide) (LiTFSI, Aldrich) anion. In a typical procedure, 10 g SiO_2-IL-Cl was dissolved in 300 ml DI water. 8 g LiTFSI salt was also dissolved in 50 ml DI water separately, and added to SiO_2-IL-Cl solution with continuous stirring. Due to the hydrophobic nature of the TFSI anion, the SiO_2-IL-TFSI immediately separates from the water phase and settle to the bottom of vessel. The resultant SiO_2-IL-TFSI was harvested from solution by repeated washing with DI water and centrifugation, and finally dried. The product was re-dispersed in acetone to remove the partially exchanged Cl-anion silica nanoparticles, and then lyophilized under vacuum to remove the final traces of water. Fig. 1(b) is a TEM micrograph for the material, which confirms its nano-particulate nature and clearly shows the effectiveness of the surface functionalization in limiting nanoparticle aggregation.

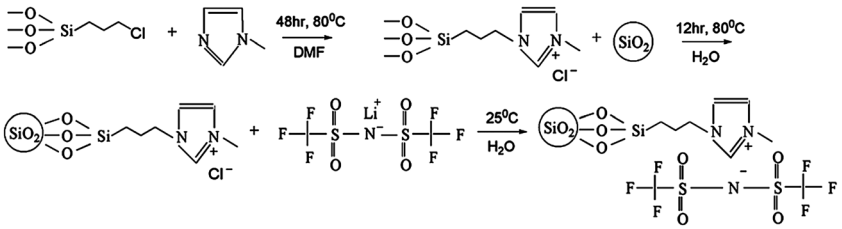

Scheme 1 Synthesis method used for creating SiO_2-IL-TFSI.

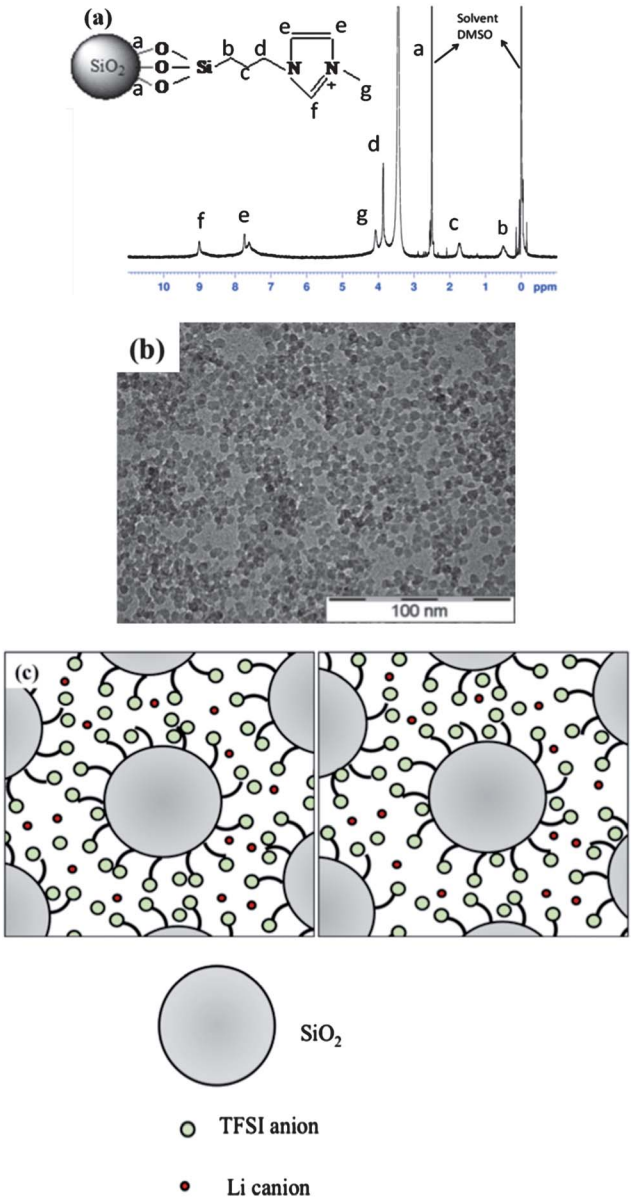

Fig. 1 (a) H-NMR spectra for SiO_2-IL-Cl in DMSO. (b) Transmission electron micrograph of SiO_2-IL-TFSI deposited from solution on to a carbon grid. (c) Schematic of ion distribution in SiO_2-IL-TFSI/LiTFSI electrolytes illustrating particle-induced ion dissociation—gray circles represent impermeable particles; green and red dots represent the TFSI anions and lithium cations, respectively. The immobile particle surfaces or the cations tethered to the surface absorb TFSI and promote ion-pair dissociation in LiTFSI.

Preparation of SiO_2-IL-TFSI/LiTFSI mixtures. Both SiO_2-IL-TFSI and LiTFSI salt were dissolved separately in acetone. The desired amount of SiO_2-IL-TFSI solution was added to the LiTFSI solution, and the mixtures were sonicated to form a uniform phase. The samples were subsequently dried at 50 °C for 2 days and the final traces of water removed by drying for another 2 days in a vacuum oven at 45 °C. Fig. 1(c) is a schematic representation of the SiO_2-IL-TFSI/LiTFSI mixture.

Characterization

Transmission electron microscopy (TEM) was used to characterize the SiO_2-IL-TFSI/LiTFSI electrolytes. TEM images were recorded at 120 kV with a FEI TECNAI T-12 TWIN TEM. Samples were dissolved in acetone and dropped onto 600 mesh copper grids to perform the TEM measurements. A Seiko Instrument TG-DTA6200 under N_2 flow and TA Instrument DSC Q2000 were used for thermal analysis. X-Ray diffraction was examined under mylar film with a Rigaku Ultima VI powder X-ray diffractometer with Cu-Kα radiation ($K_{\alpha1}$, $\lambda = 1.5406$ Å and $K_{\alpha2}$, $\lambda = 1.5444$ Å).

Ionic conductivity of the SiO_2-IL-TFSI/LiTFSI electrolytes was characterized using a Novocontrol N40 broadband dielectric spectrometer. DC ionic conductivity values were extracted from this data using a standard procedure (see Figure S2, supporting information†). Rheology measurements were performed with an Paar Physica MCR 501 and a Rheometrics Scientific ARES rheometer equipped with 10 mm and 25 mm cone-and-plate fixtures. The electrochemical stability window was examined using a Solartron (Model 1470) Potentiostat/Galvanostat in a symmetric lithium metal coin cell configuration at a scan rate of 1 mV s^{-1}. The lithium transference number was also determined using the Solartron Potentiostat/Galvanostat with a step voltage of 5mV and a Solartron Frequency Response Analyzer (Model 1252).

Results and discussion

Physical properties of SiO_2-IL-TFSI/LiTFSI mixtures were characterized using TG-DTA and DSC and the results summarized in the supporting information section (see Figures S3 and S4). These results show that the mixtures exhibit thermal stability up to and above 400 °C, and that thermal stability increases with increasing content of SiO_2-IL-TFSI. DSC analysis also shows that the glass transition temperature (T_g) of the mixtures increased with increased doping of LiTFSI. The pure SiO_2-IL-TFSI has a T_g of −78 °C, a SiO_2-IL-TFSI/LiTFSI mixture with 50 wt% SiO_2-IL-TFSI exhibits a T_g of −73 °C; and for a mixture with 5 wt% SiO_2-IL-TFSI, T_g increased to −55 °C.

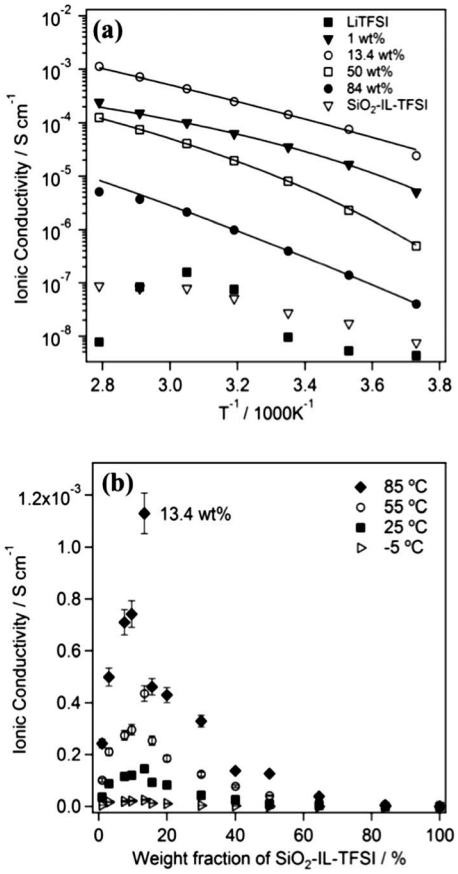

Fig. 2 **(a)** Ionic conductivities of various weight fractions of SiO_2-IL-TFSI in SiO_2-IL-TFSI/LiTFSI blends as a function of temperature. The solid lines in the figure are the VFT fits for the temperature-dependent ionic conductivity. **(b)** Isothermal ionic conductivities of SiO_2-IL-TFSI/LiTFSI systems as a function of SiO_2-IL-TFSI weight fraction.

The ionic conductivity of the SiO_2-IL-TFSI electrolytes is presented in Fig. 2(a) as a function of temperature and LiTFSI loading. The experimental data is fit by a VFT form, $\sigma = A\exp(-B/(T - T_0))$, where A is the pre-exponential factor, for the range of temperature studied, B is the effective activation energy barrier for coupled ions and local segment motion in thermal units, and T and T_0 are the measurement and reference temperatures, respectively. The VFT parameters are summarized in Table S1 for all of the materials used in the study. It should be noted that VFT-like temperature-dependent ionic conductivities are found in electrolytes where local segmental motion, chain relaxation, and crystallinity play important roles. And the motion of the ions themselves from one electrolyte site to another is of minor importance.[37] Although perhaps expected for systems such as ours, where the chain length of the tethered ionic liquid is small compared with the diameter of particle core, the VFT dependence implies that the ionic conductivity of the SiO_2-IL-TFSI/LiTFSI mixtures can be understood in terms of local segmental and breathing motions of molecules in the materials.

Fig. 2(b) shows the effect of LiTFSI composition on the isothermal ionic conductivity. It is apparent from the figure that the ionic conductivity of all mixtures is significantly enhanced over the pure components throughout the examined temperature range. Notably, the figure shows that the isothermal conductivities of SiO_2-IL-TFSI/LiTFSI mixtures exhibit a pronounced maximum, with mixtures containing 13.4wt% SiO_2-IL-TFSI displaying the highest ionic conductivity. At room temperature, the ionic conductivity of the 13.4wt% SiO_2-IL-TFSI mixture is approximately 10^{-4} S cm^{-1}, which is more than three orders of magnitude higher than that of either of the pure components. It is also apparent from the data in Table S1 that the pre-exponential factor A also exhibits a maximum with increasing SiO_2-IL-TFSI content in the electrolyte, whereas the two other parameters, B and T_0, do not exhibit any well-defined trend. This implies that the principal source of the conductivity increase upon addition of SiO_2-IL-TFSI is an effectively higher concentration of mobile ions in the electrolyte.

Fig. 3(a) and 3(b) report mechanical properties of the SiO_2-IL-TFSI/LiTFSI mixtures over the same range of SiO_2-IL-TFSI compositions where the maximum ionic conductivity is observed. The figure shows that the materials exhibit distinctive solid-like rheological properties, wherein the elastic/storage modulus, G', is substantially larger than the viscous/loss modulus G''. The figure further shows that both G' and G'' become larger as the SiO_2-IL-TFSI content is increased, which is consistent with normal expectations for polymer-particle hybrids and with results reported in our previous studies of nanoparticle-hybrid

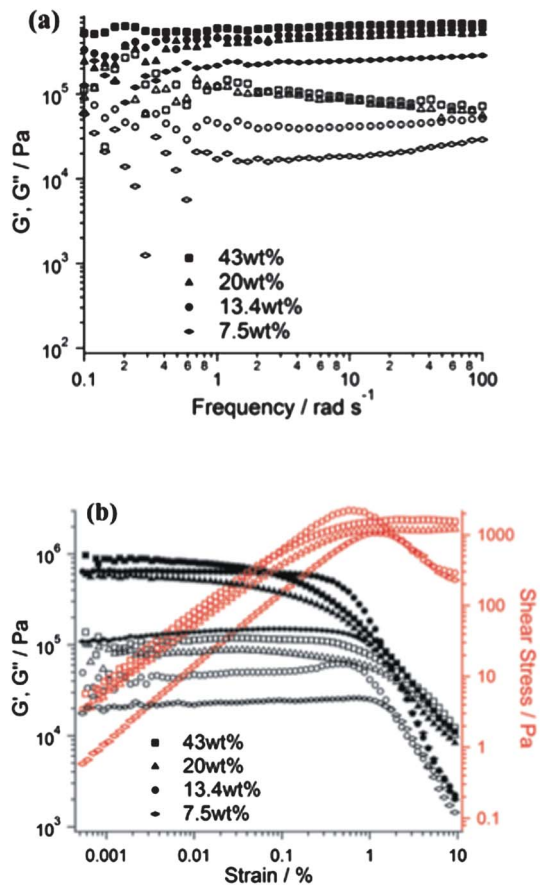

Fig. 3 **(a)** Storage modulus G' (filled symbols) and loss modulus G'' (open) of various wt% SiO_2-IL-TFSI/LiTFSI as a function of angular frequency under fixed strain 0.01%. **(b)** Storage modulus G', loss modulus G'' and shear stress as a function of shear strain at a fixed angular frequency of 10 rad s^{-1}.

electrolytes.[36,38,39] Finally, Fig. 3(a) shows that both moduli are at most weak functions of the strain frequency (deformation rate) and that the dependence becomes weaker as the SiO_2-IL-TFSI content is increased. These observations are consistent with the idea that the electrolytes become more solid-like as the nanoparticle loading is increased and the particles become jammed.[40]

Fig. 3(b) shows that at low shear strains, G' and G'' are independent of strain, and $G' > G''$, characteristics of a solid-like, linear elastic material. However, upon application of sufficient levels of strain, the electrolytes yield and transition to a regime where the shear stress (right axis) exhibits a pronounced change of slope characteristic of yielding and plastic flow. For the materials containing 7.5 wt% and 13.4 wt% SiO_2-IL-TFSI, the yielding transition is accompanied by a noticeable maximum in G''. This maximum has been reported previously to be a characteristic of a class of materials termed soft glasses;[41–43] it is believed to originate from breakage of cages provided by surrounding particles that jam motion of any given particle in the hybrids. This feature of the electrolytes is important for practical reasons; it indicates that while they might be solid-like under normal battery operating conditions (zero strain) they can be processed into complex shapes by application of strain. It also means that under normal battery operating conditions, the hybrid SiO_2-IL-TFSI particles will not move, and as such can serve as an immobile source or sink for TFSI ions.

A similar maximum conductivity has been reported in "soggy sand" hybrid electrolytes as the particle content rises.[44] Even in this context, a rising conductivity with particle loading is unexpected because the viscosity of the electrolyte should rise as the particle content increases and the system loses free-volume for ion transport. Bhattacharyya and Maier introduced the concept of adsorption-induced electrolyte polarization to explain their observations.[44] Specifically, the authors contend that an increasing ionic conductivity with particle loading arises because interactions between ions in solution and charged species on the particle surface weaken ion pair interactions in the electrolytes, which enhances ion mobility. Because there is a finite number of dissociable ions in solution, the conductivity increase produced by polarization should saturate beyond a critical particle loading, and should eventually give way to the more usual tendency of particles to decrease void fraction, which increases viscosity and reduces conductivity. Taken together, the two factors (rising ion mobility due to particle-induced polarization and falling ion mobility due to increasing suspension viscosity) nicely explain the conductivity maximum in soggy-sand hybrid electrolytes.

A similar particle-induced polarization mechanism might be used to understand the conductivity maximum observed for the SiO_2-IL-TFSI/TFSI systems. Specifically, the bulky TFSI anion in the LiTFSI can associate with the particle-tethered cation, allowing the associated lithium ions to move more freely in response to an imposed field. Because the enhanced conductivity produced by this mechanism originates from enhanced mobility of the lithium ion, it should not only exhibit a maximum as the particle content rises, but should also be accompanied by an enhancement in T_{Li^+}. To evaluate this hypothesis, T_{Li^+} for the electrolytes was determined at room temperature using the method of Bruce[45] and Scrosati[46] (see Supporting Information, Figure S5). Our results nicely show that whereas the SiO_2-IL-TFSI/LiTFSI with 13.4 wt% SiO_2-IL-TFSI has a $T_{Li^+} = 0.54$, materials with 7.5 wt% and 20 wt% SiO_2-IL-TFSI exhibit measurably lower T_{Li^+} values of 0.33 and 0.21, respectively. These transference numbers are all notably larger than reported T_{Li^+} values for untethered IL electrolytes, directly attesting to the benefits of tethering the IL. We suspect that the same physics exist in the ZrO_2 hybrid IL electrolytes reported previously,[24] and that the particle-induced polarization concept should be broadly useful for tuning T_{Li^+} of tethered electrolytes based on ILs.

Significant evidence that interactions between TFSI ions in LiTFSI and the tethered IL are strong and long-range comes from X-ray diffraction (XRD) analysis. Fig. 4 reports XRD data for LiTFSI, SiO_2-IL-TFSI and mixtures with compositions that bracket those where the conductivity maximum is observed. It is apparent from the figure that while LiTFSI is a crystalline solid and SiO_2-IL-TFSI is completely disordered at the conditions of the measurements, the mixtures exhibits intermediate levels of ordering. In particular, the intensities and positions of the diffraction peaks change as the content of SiO_2-IL-TFSI in the mixtures is increased. For example, the diffraction maxima at 2q values around 33 degrees are seen to initially increase relative to the baseline LiTFSI, but ultimately the intensity of all diffraction peaks are completely depressed as the SiO_2-IL-TFSI content is increased over 20 wt%.

This observation means that the presence of SiO_2-IL-TFSI in the mixtures depresses crystallization of LiTFSI and is the likely source of the liquid-like consistency of the mixtures at intermediate nanoparticle loadings. Consistent with the discussion in the previous section, it also implies that the effect of the particles on association of lithium and TFSI ions is greatest at a SiO_2-IL-TFSI content near 20 wt%. We speculate that this behavior stems from interactions between the surface-tethered cations and TFSI ions associated with the LiTFSI salt (see Fig. 1c). However, as illustrated in Fig. 1c, we cannot rule out the synergistic effect produced by adsorption of the TFSI ions to exposed un-functionalized sites on the SiO_2 nanoparticle cores. Work is ongoing to assess the effect of the IL-TFSI grafting density on the size of the conductivity maximum and on the growth rate and structure of lithium dendrites generated by cycling the symmetric lithium cells.

In closing, we point out that the electrochemical stability of the 13.4wt% SiO_2-IL-TFSI/ LiTFSI hybrid electrolyte is also

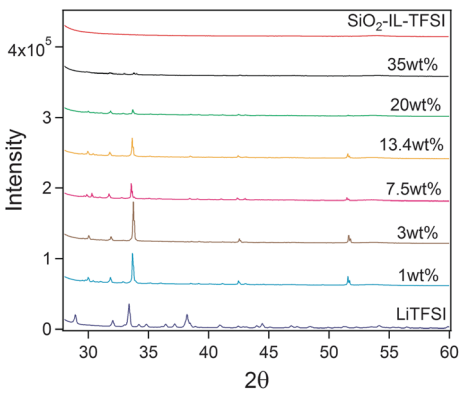

Fig. 4 Results from X-ray diffraction analysis of hybrid SiO_2-IL-TFSI/LiTFSI electrolyte systems containing varying weight fractions of SiO_2-IL-TFSI. XRD profiles for the pure SiO_2-IL-TFSI and LiTFSI are provided as reference.

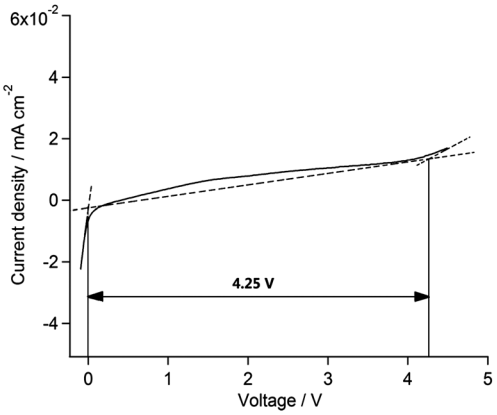

Fig. 5 *I–V* diagram obtained from linear-sweep voltammetry of 13.4 wt % SiO_2-IL-TFSI/LiTFSI in a symmetric lithium metal cell. The measurement was performed at a scan rate of 1 mV s^{-1} and at room temperature.

attractive. Specifically, the stability window of the electrolyte that exhibits the largest ionic conductivity was characterized using linear sweep voltammetry in a symmetric lithium coin cell at room temperature (Fig. 5). The material is seen to display an EW of around 4.25V *vs.* Li/Li^+. This stability has been confirmed using cyclic voltammetry (Figure S6), which shows that following the 1st cycle, the materials exhibit repeatable *I–V* curves for the following nine cycles.

Conclusions

We report on the synthesis and characterization of novel organic-inorganic hybrid electrolytes comprised of ionic liquid-tethered silica nanoparticles dispersed in the salt LiTFSI. We find that addition of SiO_2-IL-TFSI to LiTFSI reduces ordering of ions in the salt, and over a range of particle concentrations yields a hybrid electrolyte that displays an ionic conductivity maximum. In the range of particle concentrations where the maximum is observed, the electrolytes exhibit depressed X-ray diffraction maxima and display soft-glassy solid rheology indicative of a jammed material. We hypothesize that at intermediate nanoparticle loadings interactions between the TFSI counterion of the salt and the tethered cation of the IL surface disrupt crystallization of LiTFSI, simultaneously improving lithium ion mobility, lithium ion transference number, and mechanical properties of the electrolytes. An additional attractive feature of the new hybrid electrolytes is that the jammed SiO_2-IL-TFSI provides a fixed, uniform reservoir of anions throughout the electrolyte, which we anticipate will emerge as an important strategy for suppressing formation of a space charge and lithium dendrite growth in secondary lithium batteries that employ metallic lithium as the anode.

Acknowledgements

This publication was based on work supported in part by Award No. KUS-C1-018-02, made by King Abdullah University of Science and Technology (KAUST) and by the National Science Foundation, Award No. DMR-1006323. Facilities available through the Cornell Center for Materials Research (CCMR), National Science Foundation Award No. DMR-1120296, were also used for this study.

Notes and references

1 J. M. Tarascon and M. Armand, *Nature*, 2001, **414**, 359.
2 R. Fong, U. Vonsacken and J. R. Dahn, *J. Electrochem. Soc.*, 1990, **137**, 2009.
3 Y. Idota, T. Kubota, A. Matsufuji, Y. Maekawa and T. Miyasaka, *Science*, 1997, **276**, 1395.
4 J. Hassoun, S. Panero, P. Simon, P. L. Taberna and B. Scrosati, *Adv. Mater.*, 2007, **19**, 1632.
5 L. Taberna, S. Mitra, P. Poizot, P. Simon and J. M. Tarascon, *Nat. Mater.*, 2006, **5**, 567.
6 K. Kang, Y. S. Meng, J. Breger, C. P. Grey and G. Ceder, *Science*, 2006, **311**, 977.
7 M. Yoshio, R. J. Brodd, and A. Kozawa, (Eds), *Lithium-Ion Batteries: Science & Technologies*. Springer, 2009.
8 D. Linden and T. B. Reddy, *Handbook of Batteries*, 3rd Edition, McGraw-Hill, 2002.
9 J. Yamaki, S. Tobishima, K. Hayashi, K. Saito, Y. Nemoto and M. Arakawa, *J. Power Sources*, 1998, **74**, 219.
10 R. Bhattacharyya, B. Key, H. Chen, A. S. Best, A. F. Hollenkamp and C. P. Grey, *Nat. Mater.*, 2010, **9**, 504.
11 J.-N. Chazalviel, *Phys. Rev. A: At., Mol., Opt. Phys.*, 1990, **42**, 7355.
12 M. Rosso, T. Gobron, C. Brissot, J.-N. Chazalviel and S. Lascaud, *J. Power Sources*, 2001, **97–98**, 804.
13 M. Armand, F. Endres, D. R. MacFarlane, H. Ohno and B. Scrosati, *Nat. Mater.*, 2009, **8**, 621.
14 F. Zhou, Y. Liang and W. Liu, *Chem. Soc. Rev.*, 2009, **38**, 2590.
15 J. Lua, F. Yana and J. Texter, *Prog. Polym. Sci.*, 2009, **34**, 431.
16 R. E. Morris, *Chem. Commun.*, 2009, 2990.
17 B. Scrosati and J. Garche, *J. Power Sources*, 2010, **195**, 2419.
18 A. Lewandowski and A. S. Widerska-Mocek, *J. Power Sources*, 2009, **194**, 601.
19 G. H. Lane, P. M. Bayley, B. R. Clare, A. S. Best, D. R. MacFarlane, M. Forsyth and A. F. Hollenkamp, *J. Phys. Chem. C*, 2010, **114**, 21775.
20 R. E. Baltus, B. H. Culbertson, S. Dai, H. Luo and D. W. DePaoli, *J. Phys. Chem. B*, 2004, **108**, 721.
21 P. B. Webb, T. E. Kunene and D. J. Cole-Hamilton, *Green Chem.*, 2005, **7**, 373.
22 A. Ispas, B. Adolphi, A. Bund and F. Endres, *Phys. Chem. Chem. Phys.*, 2010, **12**, 1793.
23 K. Kodama, R. Tsuda, K. Niitsuma, T. Tamura, T. Ueki, H. Kokubo and M. Watanabe, *Polym. J.*, 2011, **43**, 242.
24 G. Dlubek, Y. Yu, R. Krause-Rehberg, W. Beichel, S. Bulut, N. Pogodina, I. Krossing and Ch. Friedrich, *J. Chem. Phys.*, 2010, **502**, 124.
25 D. Xiao, L. G. Hines, M. W. Holtz, K. Song, R. A. Bartsch and E. L. Quitevis, *Chem. Phys. Lett.*, 2010, **497**, 37.
26 J.-K. Kim, A. Matic, A. J.-H. Ahn and P. Jacobsson, *J. Power Sources*, 2010, **195**, 7639.
27 S. Duluard, J. Grondin, J.-L. Bruneel, I. Pianet, A. Grelard, G. Campet, M.-H. Delville and J.-C. Lassegues, *J. Raman Spectrosc.*, 2008, **39**, 627.
28 Y. Saito, T. Umecky, J. Niwa, T. Sakai and S. Maeda, *J. Phys. Chem. B*, 2007, **111**, 11794.
29 T. Frömling, M. Kunze, M. Schonhoff, J. Sundermeyer and B. Roling, *J. Phys. Chem. B*, 2008, **112**, 12985.
30 P. Wang, S. M. Zakeeruddin, P. Comte, I. Exnar and M. Gratzel, *J. Am. Chem. Soc.*, 2003, **125**, 1166.
31 S. Saito, Y. Katoh, H. Kokubo, M. Watanabe and S. Maruo, *J. Micromech. Microeng.*, 2009, **19**, 035005.
32 K. Ueno, A. Inaba, T. Ueki, M. Kondoh and M. Watanabe, *Langmuir*, 2010, **26**, 18031.
33 K. Ueno, Y. Sano, A. Inaba, M. Kondoh and M. Watanabe, *J. Phys. Chem. B*, 2010, **114**, 13095.
34 K. Ueno, K. Hata, T. Katakabe, M. Kondoh and M. Watanabe, *J. Phys. Chem. B*, 2008, **112**, 9013.
35 S. Long, P. C. Howlett, D. R. MacFarlane and M. Forsyth, *Solid State Ionics*, 2006, **177**, 647.

36 S. S. Moganty, N. Jayaprakash, J. L. Nugent, J. Shen and L. A. Archer, *Angew. Chem., Int. Ed.*, 2010, **49**, 9158.
37 J. B. Kerr, S. E. Sloop, G. Liu, Y. B. Han, J. Hou and S. Wang, *J. Power Sources*, 2002, **110**, 389.
38 J. L. Schaefer, S. S. Moganty, D. A. Yanga and L. A. Archer, *J. Mater. Chem.*, 2011, **21**, 10094.
39 J. L. Nugent, S. S. Moganty and L. A. Archer, *Adv. Mater.*, 2010, **22**, 3677.
40 V. Trappe, V. Prasad, L. Cipelletti, P. N. Segre and D. A. Weitz, *Nature*, 2001, **411**, 772.
41 P. Sollich, F. Lequeux, P. Hébraud and M. E. Cates, *Phys. Rev. Lett.*, 1997, **78**, 2020.
42 P. Agarwal, H. Qi and L. A. Archer, *Nano Lett.*, 2010, **10**, 111.
43 P. Agarwal, S. Srivastava and L. A. Archer, *Phys. Rev. Lett.*, 2011, **107**, 268302.
44 A. J. Bhattacharyya and J. Maier, *Adv. Mater.*, 2004, **16**, 9.
45 P. G. Bruce, J. Evans and C. A. Vincent, *Solid State Ionics*, 1988, **28–30**, 918.
46 G. B. Appetecchi, G. Dautzenberg and B. Scrosati, *J. Electrochem. Soc.*, 1996, **143**, 6.

